CHALMERS | UNIVERSITY OF GOTHENBURG

PREPRINT 2008:34

Model Adaptivity for Elasticity on Thin Domains

DAVID HEINTZ

Department of Mathematical Sciences
Division of Mathematics
CHALMERS UNIVERSITY OF TECHNOLOGY
UNIVERSITY OF GOTHENBURG
Göteborg Sweden 2008

Preprint 2008:34

Model Adaptivity for Elasticity on Thin Domains

David Heintz

Department of Mathematical Sciences
Division of Mathematics
Chalmers University of Technology and University of Gothenburg
SE-412 96 Göteborg, Sweden
Göteborg, October 2008

Preprint 2008:34
ISSN 1652-9715

Matematiska vetenskaper
Göteborg 2008

Model Adaptivity for Elasticity on Thin Domains

David Heintz

Department of Mathematical Sciences
Chalmers University of Technology and University of Gothenburg
SE-412 96 Göteborg

Abstract

We consider the equations of linear elasticity on thin domains in two spatial dimensions. The main idea is the construction of a model hierarchy, that facilitates an efficient solution procedure. An energy norm *a posteriori* error estimate is outlined, which provides an upper bound on the total error. However, and more important, a preceding semi-discrete estimate motivates uncoupling of the discretization and model errors—thereby we obtain a means for extracting local error indicators. We introduce an adaptive algorithm, which concurrently refines mesh and model, aiming at a balance between different error contributions. Numerical results are presented to exemplify the behavior of the algorithm.

Keywords: *model adaptivity, model error, a posteriori error*

1 Introduction

Adaptive techniques based on a posteriori error estimates in the finite element method (FEM) are well-developed. The algorithms usually strive to efficiently reduce the discretization error, meaning the discrepancy between the continuous model—the exact solution of the differential equation at hand—and the corresponding FE-solution. The goal is to ascertain a user-specified tolerance on the error to a (nearly) minimal computational cost.

However, if the prescribed accuracy should be with respect to the total error, one has to consider the choice of model carefully. The total error e_{T} is

$$e_{\mathrm{T}} = e_{\mathrm{D}} + e_{\mathrm{M}},$$

including the model error e_{M}. Unfortunately, the most complex model (thus implying $e_{\mathrm{M}} \to 0$) could be inherently expensive to use, just as resolving a simpler one ($e_{\mathrm{D}} \to 0$) does not improve the accuracy, once the relatively large e_{M} dominates. Therefore we seek an adaptive strategy taking both error sources into account. Ideally, the local error contributions should be balanced, by refining the computational mesh and the model concurrently, which is known as *model adaptivity*.

In this paper we apply model adaptivity to the equations of linear elasticity in 2D on thin domains, where, given $\boldsymbol{x} = (x_1, x_2)$, x_2 is understood as the thin direction. This requires an available hierarchy of models, and such reduced models—as compared to the linear elasticity theory—are typically obtained using simplified deformation relations, e.g., the Bernoulli and Timoshenko beam theories. We shall instead follow Babuška, Lee and Schwab [2], and employ a model hierarchy based on increasingly higher polynomial expansions through the thickness of the domain, coupled with a Galerkin approach. However, we make no assumptions on the discretization error being negligible, and thus strive for simultaneous a posteriori estimation of both discretization and modeling errors.

For a certain polynomial expansion $\boldsymbol{q}$, we emphasize that the dimension of the problem could be reduced, if the x_2-dependence of the weak FE-formulation is integrated. The resulting boundary value problem, a system of ordinary differential equations (ODEs), for any $\boldsymbol{q}$, is said to correspond to a particular model. The kinematic assumptions would rely on a minimization principle, since Galerkin's method corresponds to minimizing the potential energy, together with a prescribed polynomial dependence of the displacements in the thin direction.

This viewpoint contrasts that of regarding the polynomial expansion as purely algorithmic, a certain simplified *hp*-refinement process (with separated *h*- and *p*-refinements in the x_1- and x_2-directions respectively), which instead attributes the model error to a discretization error. In the literature this kind of model adaptivity is known as *q*-adaptivity, which consequently becomes *hq*-adaptivity, when used in conjunction with *h*-adaptivity for the FE-discretization.

The reason for implementing the thin domain problem in a higher dimension, is to obtain a straightforward means for estimating e_{M}, information that is used for changing the underlying model locally.

The proposed model hierarchy will be a natural extension to another hierarchy, by bridging the abovementioned beam theories and the linear elasticity theory. This is shown by a simple example to conclude Section 3, once the relevant equations have been introduced.

We derive an energy norm a posteriori error estimate (31), based on orthogonality relations and interpolation theory, that is an upper bound of the total error.

A semi-discrete error estimate (30) justifies splitting the total error in two distinct parts, representing the effects of the discretization and model errors. It thus becomes the cornerstone for an adaptive algorithm (Algorithm 1), which strives to balance the local error contributions. Consecutive updates of mesh and model are governed by (42) and (43), local error indicators derived using a residual-based approach (with respect to the complete solution space).

In brief the paper consists of the following parts: in Section 2 we present the model problem and its corresponding weak and finite element formulations; next, in Section 3, follows a review of beam theory; in Section 4 the a posteriori error estimate is derived; and finally, in Section 5, we propose the framework of an adaptive algorithm and present some numerical results.

2 A Finite Element Method for Navier's Equations

Consider a thin rectangular domain $\Omega \subset \mathbb{R}^2$, representing a deformable medium subjected to external loads. These include body forces $\boldsymbol{f}$ and surface tractions $\boldsymbol{g}$, causing deformations of the material, which we describe by the following model problem: Find the displacement field $\boldsymbol{u} = (u_1, u_2)$ and the symmetric stress tensor $\boldsymbol{\sigma} = (\sigma_{ij})_{i,j=1}^2$, such that

$$\begin{aligned}
\boldsymbol{\sigma}(\boldsymbol{u}) &= \lambda \operatorname{div}(\boldsymbol{u})\, \boldsymbol{I} + 2\mu\boldsymbol{\varepsilon}(\boldsymbol{u}) && \text{in } \Omega && (1)\\
-\operatorname{div}(\boldsymbol{\sigma}) &= \boldsymbol{f} && \text{in } \Omega && (2)\\
\boldsymbol{u} &= \boldsymbol{0} && \text{on } \partial\Omega_{\mathrm{D}} &&\\
\boldsymbol{\sigma}\cdot\boldsymbol{n} &= \boldsymbol{g} && \text{on } \partial\Omega_{\mathrm{N}} &&
\end{aligned}$$

where $\partial\Omega = \partial\Omega_{\mathrm{D}} \cup \partial\Omega_{\mathrm{N}}$ is a partitioned boundary of Ω. Let the Lamé coefficients

$$\lambda = \frac{E\nu}{(1+\nu)(1-2\nu)}, \quad \mu = \frac{E}{2(1+\nu)}, \tag{3}$$

with E and ν being Young's modulus and Poisson's ratio, respectively. Furthermore, $\boldsymbol{I}$ is the identity tensor, $\boldsymbol{n}$ denotes the outward unit normal to $\partial\Omega_{\mathrm{N}}$, and the strain tensor is

$$\boldsymbol{\varepsilon}(\boldsymbol{u}) = \tfrac{1}{2}\big(\nabla\boldsymbol{u} + \nabla\boldsymbol{u}^{\mathrm{T}}\big).$$

The vector-valued tensor divergence is

$$\mathrm{div}(\boldsymbol{\sigma}) = \left(\sum_{j=1}^{2} \frac{\partial\sigma_{ij}}{\partial x_j}\right)_{i=1}^{2},$$

representing the internal forces of the equilibrium equation. This formulation assumes, firstly, a constitutive relation corresponding to linear isotropic elasticity (the material properties are the same in all directions), with stresses and strains related by

$$\boldsymbol{\sigma}_{\mathrm{v}} = \begin{bmatrix}\sigma_{11}\\ \sigma_{22}\\ \sigma_{12}\end{bmatrix} = \begin{bmatrix}D_{11} & D_{12} & D_{13}\\ D_{21} & D_{22} & D_{23}\\ D_{31} & D_{32} & D_{33}\end{bmatrix}\begin{bmatrix}\varepsilon_{11}\\ \varepsilon_{22}\\ \varepsilon_{12}\end{bmatrix} = \boldsymbol{D}(\lambda,\,\mu)\boldsymbol{\varepsilon}_{\mathrm{v}},$$

referred to as *Hooke's generalized law*. If the material is homogeneous, $\boldsymbol{D}$ becomes independent of position. Secondly, a state of plain strain prevails, i.e., the only non-zero strain components are ϵ_{11}, ϵ_{22} and ϵ_{12}. This situation typically occurs for a long and thin body, loaded by forces invariant and perpendicular to the longitudinal axis, and restricted from movement along its length [11, Chapter 12.2.1]. Lastly, we make the assumption of $\boldsymbol{u}$ belonging to a tensor-product space

$$\boldsymbol{u} = \big(\phi_1(x_1)\psi_1(x_2), \phi_2(x_1)\psi_2(x_2)\big), \tag{4}$$

i.e., the solution components are products of two functions with separated spatial dependence. The tensor-product Lagrangian finite elements, which are introduced in Section 5.2, yield FE-solutions $\boldsymbol{u}^h$ on this form. The reason for considering such solutions, is for the straightforward construction of a model hierarchy, where the displacement field has a prescribed polynomial dependence in the thin direction.

Next, relating to (4), we introduce the function spaces

$$V_\phi \otimes V_\psi = \left\{\boldsymbol{v} = (\phi_1\psi_1,\, \phi_2\psi_2) :\ \phi_i\psi_i \in V \cap H^2\right\},$$
$$V = \left\{w :\ w \in H^1,\ w|_{\partial\Omega_{\mathrm{D}}} = 0\right\},$$

where $\phi_i = \phi_i(x_1)$, $\psi_i = \psi_i(x_2)$, $H^k = H^k(\Omega)$ and $i,\, k = 1,\, 2$. The equilibrium equation (2) is multiplied by a test function $\boldsymbol{v} = (v_1,\, v_2) \in V_\phi \otimes V_\psi$, and the inner products are integrated (by parts) over the domain. Having reached thus far, we pose the following weak formulation: Find $\boldsymbol{u} \in V_\phi \otimes V_\psi$ such that

$$a(\boldsymbol{u}, \boldsymbol{v}) = L(\boldsymbol{v}), \quad \forall \boldsymbol{v} \in V_\phi \otimes V_\psi, \tag{5}$$

where the bilinear form

$$a(\boldsymbol{u}, \boldsymbol{v}) = \int_\Omega \boldsymbol{\sigma}(\boldsymbol{u}) : \boldsymbol{\varepsilon}(\boldsymbol{v})\,\mathrm{d}\boldsymbol{x} \tag{6}$$

is the integrated tensor contraction

$$\boldsymbol{\sigma} : \boldsymbol{\varepsilon} \stackrel{\mathrm{def}}{=} \sum_{i,j=1}^{2} \sigma_{ij}\varepsilon_{ij},$$

and the linear functional of the right-hand side is

$$L(\boldsymbol{v}) = (\boldsymbol{f}, \boldsymbol{v}) + (\boldsymbol{g}, \boldsymbol{v})_{\partial\Omega_{\mathrm{N}}} = \int_{\Omega} \boldsymbol{f} \cdot \boldsymbol{v} \, \mathrm{d}\boldsymbol{x} + \int_{\partial\Omega_{\mathrm{N}}} \boldsymbol{g} \cdot \boldsymbol{v} \, \mathrm{d}s. \tag{7}$$

Remark. An equivalent formulation of (5), mainly due to the symmetry and positive definiteness of the bilinear form (we refer to [5] for more details), comes in the guise of a minimization problem: Find $\boldsymbol{u} \in V_\phi \otimes V_\psi$ such that

$$F(\boldsymbol{u}) \leq F(\boldsymbol{w}), \quad \forall \boldsymbol{w} \in V_\phi \otimes V_\psi,$$

where

$$F(\boldsymbol{u}) = \tfrac{1}{2} a(\boldsymbol{u}, \boldsymbol{u}) - L(\boldsymbol{u}), \tag{8}$$

is recognized as the potential energy of $\boldsymbol{u}$.

For the numerical approximation of (5), we shall need a discrete counterpart, and as such establish a finite element method. To simplify its formulation we define the kinematic relation

$$\boldsymbol{\varepsilon}_{\mathrm{v}}(\boldsymbol{u}) = \begin{bmatrix} \frac{\partial}{\partial x_1} & 0 \\ 0 & \frac{\partial}{\partial x_2} \\ \frac{\partial}{\partial x_2} & \frac{\partial}{\partial x_1} \end{bmatrix} \begin{bmatrix} u_1 \\ u_2 \end{bmatrix} = \tilde{\boldsymbol{\nabla}} \boldsymbol{u},$$

and specify the constitutive matrix

$$\boldsymbol{D} = \begin{bmatrix} \lambda + 2\mu & \lambda & 0 \\ \lambda & \lambda + 2\mu & 0 \\ 0 & 0 & \mu \end{bmatrix},$$

for the purpose of rewriting the bilinear form as

$$a(\boldsymbol{u}, \boldsymbol{v}) = \int_{\Omega} \boldsymbol{\varepsilon}_{\mathrm{v}}(\boldsymbol{u})^{\mathrm{T}} \boldsymbol{D} \boldsymbol{\varepsilon}_{\mathrm{v}}(\boldsymbol{v}) \, \mathrm{d}\boldsymbol{x},$$

which facilitates implementation. Then we introduce a partition $\mathcal{T}_h$ of Ω, dividing the domain into N_{el} quadrilateral—suitable for tensor-product approximations—elements K_i (thus having $N_{\mathrm{ed}} = N_{\mathrm{el}} + 1$ vertical edges), such that $\mathcal{T}_h = \{K_i\}_{i=1}^{N_{\mathrm{el}}}$, with nodes $\boldsymbol{x}_i$, $i = 1, 2, \ldots, N_{\mathrm{no}}$. The function

$$h_K = \mathrm{diam}(K) = \max_{\boldsymbol{y}_1, \boldsymbol{y}_2 \in K} (\|\boldsymbol{y}_1 - \boldsymbol{y}_2\|_2), \quad \forall K \in \mathcal{T}_h,$$

represents the local mesh size, with $h = \max_{K \in \mathcal{T}_h} h_K$. Let $\mathcal{E}^h = \{E\}$ denote the set of element edges, which we split into two disjoint subsets, $\mathcal{E}^h = \mathcal{E}^h_I \cup \mathcal{E}^h_B$, namely the sets of interior and boundary edges, respectively.

The partition is associated with a function space

$$V_\phi^h \otimes V_\psi^h = \left\{ \boldsymbol{v} \in [\mathcal{C}(\Omega)]^2 : \ \boldsymbol{v}|_K \in \mathbb{Q}^2 \text{ for each } K \in \mathcal{T}_h, \, \boldsymbol{v}|_{\partial\Omega_{\mathrm{D}}} = \boldsymbol{0} \right\}, \tag{9}$$

where

$$\mathbb{Q} = \left\{ w : \ w = w_1(x_1) w_2(x_2), \, w_1 \in \mathbb{P}^1, \, w_2 \in \mathbb{P}^q \right\},$$

and $\mathbb{P}^q$ denotes the space of polynomials of degree $q \geq 1$ in one variable. A function in $V_\phi^h \otimes V_\psi^h$ is uniquely determined by its values at $\boldsymbol{x}_i$, together with the set of shape functions

$$\{\varphi_j\}_{j=1}^{N_{\text{no}}} \subset V_\phi^h \otimes V_\psi^h, \quad \varphi_j(\boldsymbol{x}_i) := \delta_j(\boldsymbol{x}_i),$$

which constitute a nodal basis for (9). It then follows that any $\boldsymbol{v} \in V_\phi^h \otimes V_\psi^h$ can be expressed as a linear combination

$$\boldsymbol{v} = \sum_{j=1}^{N_{\text{no}}} \boldsymbol{v}_j \varphi_j(\boldsymbol{x}), \tag{10}$$

where $\boldsymbol{v}_j = \boldsymbol{v}(\boldsymbol{x}_j)$ represent the nodal values of $\boldsymbol{v}$ (note that the number of degrees of freedom $N_{\text{d}} = 2N_{\text{no}}$, since the problem is vector-valued). We make an *ansatz* for a FE-solution of this type (10), and hence the FE-formulation of (5) becomes: Find $\boldsymbol{u}^h \in V_\phi^h \otimes V_\psi^h$ such that

$$a(\boldsymbol{u}^h, \boldsymbol{v}) = L(\boldsymbol{v}), \quad \forall \boldsymbol{v} \in V_\phi^h \otimes V_\psi^h, \tag{11}$$

whose solution usually is written on the standard form

$$\boldsymbol{u}^h = \begin{bmatrix} \varphi_1 & 0 & \varphi_2 & 0 & \dots \\ 0 & \varphi_1 & 0 & \varphi_2 & \dots \end{bmatrix} \begin{bmatrix} u_1^1 \\ u_2^1 \\ u_1^2 \\ u_2^2 \\ \vdots \end{bmatrix} = \boldsymbol{\varphi}\mathbf{u},$$

associating odd and even elements of $\mathbf{u}$ with displacements in x_1 and x_2, respectively. Since testing against all $\boldsymbol{v} \in V_\phi^h \otimes V_\psi^h$ reduces to testing against $\{\varphi_j\}_{j=1}^{N_{\text{no}}}$, and $\boldsymbol{\varepsilon}_{\text{v}}(\boldsymbol{u}^h) = \tilde{\boldsymbol{\nabla}}\boldsymbol{\varphi}\mathbf{u} = \boldsymbol{B}\mathbf{u}$, (11) corresponds to solving

$$\int_\Omega \boldsymbol{B}^{\text{T}}\boldsymbol{D}\boldsymbol{B}\,\mathrm{d}\boldsymbol{x}\,\mathbf{u} = \int_\Omega \boldsymbol{\varphi}^{\text{T}}\boldsymbol{f}\,\mathrm{d}\boldsymbol{x} + \int_{\partial\Omega_{\text{N}}} \boldsymbol{\varphi}^{\text{T}}\boldsymbol{g}\,\mathrm{d}s, \tag{12}$$

i.e., the matrix problem $\mathbf{S}\mathbf{u} = \mathbf{f}$, making (12) a suitable starting point for FE-implementation.

3 The Bernoulli and Timoshenko Beam Equations

The geometry of a problem sometimes allows for simplifications, although such formulations usually violate the field equations, i.e., the equilibrium balance or the kinematic and constitutive relations. Let us exemplify by considering the beam, which is dominated by its extension in the axial direction. Bernoulli stated how *"plane sections normal to the beam axis remain in that state during deformation"* (it follows that $\theta = \mathrm{d}u/\mathrm{d}x_1$, i.e., the slope of the deflection is the first order derivative). Further kinematic assumptions eventually lead to the only non-zero strain component being ϵ_{11}. Consequently, for an isotropic material with a linear elastic response, this would correspond to

$$\begin{bmatrix} \sigma_{11} \\ \sigma_{22} \end{bmatrix} = \frac{E\epsilon_{11}}{(1+\nu)(1-2\nu)} \begin{bmatrix} 1-\nu \\ \nu \end{bmatrix}, \tag{13}$$

and in particular that $\sigma_{12} = 0$, so the effects of transverse shear deformations are neglected. The constitutive relation of the Bernoulli theory is actually less complex, assuming a uniaxial

state of stress with $\sigma_{11} = E\epsilon_{11}$, suggesting that $\nu = 0$ in (13). The simplified formulation, as compared to (2), becomes a fourth order ODE (we refer to [11, Chapter 17.1] or [12, Chapter 5.9] for a detailed derivation):

$$\frac{\mathrm{d}^2}{\mathrm{d}x_1^2}\left(EI\frac{\mathrm{d}^2 u}{\mathrm{d}x_1^2}\right) = f, \tag{14}$$

where $u = u(x_1)$ and $f = f(x_1)$ represents a distributed load [$\mathtt{N/m}$]. We restrict the discussion to prismatic beams, with rectangular cross-sections of size $A = wt$, which will have a constant flexural rigidity EI [$\mathtt{Nm}^2$]. Here I [$\mathtt{m}^4$] is the moment of inertia, and with respect to unit length (set the width $w = 1$), we now get

$$I = \int_A x_2^2 \,\mathrm{d}A = \int_{-t/2}^{t/2} x_2^2 \, dx_2 = \frac{t^3}{12}.$$

Timoshenko proposed a more accurate model, which accounts for deflections due to shear. Thus a plane section normal to the beam axis, although still plane, is not necessarily normal after deformation. The system of ODEs has the form (rewritten from [12, Chapter 5.12]):

$$\begin{cases} EI\dfrac{\mathrm{d}^3\theta}{\mathrm{d}x_1^3} = f, \\ \quad \dfrac{\mathrm{d}u}{\mathrm{d}x_1} = \theta - \dfrac{EI}{A\kappa G}\dfrac{\mathrm{d}^2\theta}{\mathrm{d}x_1^2} \end{cases} \tag{15}$$

where κ represents the shear coefficient [$\mathtt{1}$] (geometry dependent), and G is the shear modulus [$\mathtt{N/m}^2$]. Should the last term of the second equation be omitted, (15) and (14) are equivalent.

The Bernoulli beam theory provides close approximations for long slender beams, typically when $L/t > 5$–10 [11, Chapter 17.1], since the shear strain σ_{12} then usually is small. Thicker beams are better modeled using the Timoshenko beam theory. For still higher beams, we now show the thin domain approach, as mentioned briefly in Section 1, to be a natural extension of the latter.

Linear polynomial dependence. Starting at (5), consider a completely fixed uniform beam of length L and thickness t, subjected to a constant volume load, $\boldsymbol{f} = [0, -a]$, $a > 0$ [$\mathtt{N/m}^2$]. If we assume a linear polynomial dependence of the displacements (in the thin direction), this model (the simplest available in our hierarchy) has the semi-discrete solution

$$\boldsymbol{u}(\boldsymbol{x}) = \begin{bmatrix} u_1(\boldsymbol{x}) \\ u_2(\boldsymbol{x}) \end{bmatrix} = \begin{bmatrix} u_1^{\mathrm{L}}(x_1)\left(1 - \frac{x_2}{t}\right) + u_1^{\mathrm{U}}(x_1)\frac{x_2}{t} \\ u_2^{\mathrm{L}}(x_1)\left(1 - \frac{x_2}{t}\right) + u_2^{\mathrm{U}}(x_1)\frac{x_2}{t} \end{bmatrix}, \quad \boldsymbol{u} \in V_\phi \otimes V_\psi^h, \tag{16}$$

where u_i^{L} and u_i^{U} denote displacements on the lower and upper sides, respectively. Moreover, when imposing the additional kinematic relations (according to the Bernoulli and Timoshenko theories)

$$u_1^{\mathrm{U}} = -u_1^{\mathrm{L}}, \quad u_2^{\mathrm{L}} = u_2^{\mathrm{U}}, \tag{17}$$

as shown in Figure 1, and assuming small deformations, so that $\theta \approx \tan(\theta) \approx u_1^{\mathrm{U}}/(t/2)$, (16) reduces to

$$\boldsymbol{u}(\boldsymbol{x}) = \begin{bmatrix} \left(x_2 - \frac{t}{2}\right)\theta \\ -u \end{bmatrix}, \tag{18}$$

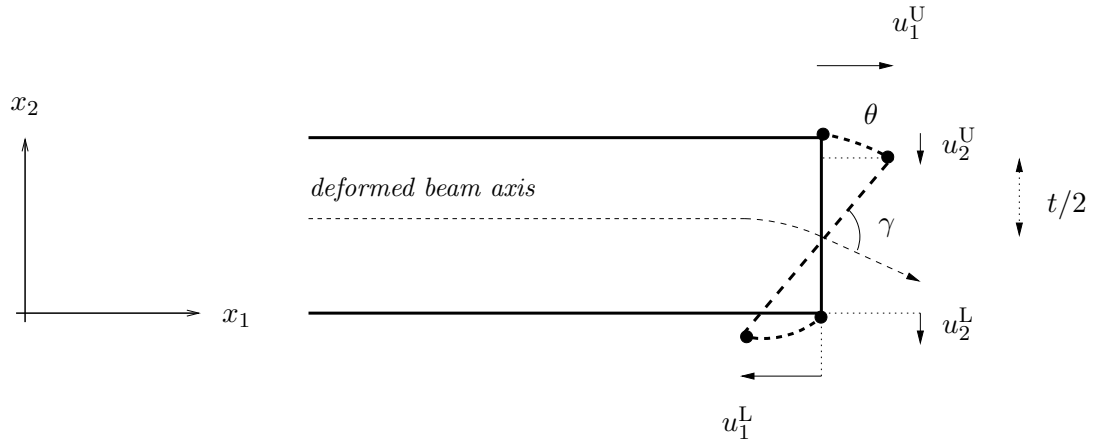

FIGURE 1: *Plane normal sections may not be normal after deformation ($\gamma < \pi/2$)*

writing $-u = u_2^{\mathrm{U}}$ for the transversal deflection. Let us substitute (18) into (5) for $\nu = 0$ (since there is no lateral contraction in the beam theory). It then follows by (3) that $\lambda = 0$, and the shear modulus

$$\mu = G = \frac{E}{2(1+\nu)} = \frac{E}{2},$$

whereas the stress tensor (1) simplifies to $\boldsymbol{\sigma}(\boldsymbol{u}) = E\boldsymbol{\varepsilon}(\boldsymbol{u})$. Next, in accordance with Galerkin's method, we test the weak form against

$$\boldsymbol{v}_1(\boldsymbol{x}) = \begin{bmatrix} v_1(x_1)\left(\frac{2}{t}x_2 - 1\right) \\ 0 \end{bmatrix}, \quad \boldsymbol{v}_2(\boldsymbol{x}) = \begin{bmatrix} 0 \\ v_2(x_1) \end{bmatrix}, \quad \boldsymbol{v}_i \in V_\phi \otimes V_\psi^h.$$

Note that the x_2-dependence of (6) can be integrated: if denoting, e.g., $\mathrm{d}u/\mathrm{d}x_1 = u'$ for short, that means

$$\begin{aligned} a(\boldsymbol{u}, \boldsymbol{v}_1) &= E\int_0^L \int_0^t \Big(\big(x_2 - \tfrac{t}{2}\big)\big(\tfrac{2}{t}x_2 - 1\big)\theta' v_1' + \tfrac{1}{t}(\theta - u')v_1 \Big)\, \mathrm{d}x_2 \mathrm{d}x_1 \\ &= E\int_0^L \Big(\tfrac{t^2}{6}\theta' v_1' + (\theta - u')v_1 \Big)\, \mathrm{d}x_1 \\ &= E\int_0^L \big((\theta - u') - \tfrac{t^2}{6}\theta'' \big) v_1 \, \mathrm{d}x_1, \end{aligned}$$

using integration by parts—assume u and θ to be sufficiently regular functions—in conjunction with the prescribed boundary conditions (we have neither translation nor rotation at the fixed ends $x_1 = 0$, $x_1 = L$). Analogously, for the second test function,

$$\begin{aligned} a(\boldsymbol{u}, \boldsymbol{v}_2) &= E\int_0^L \int_0^t \tfrac{1}{2}(\theta - u')v_2' \, \mathrm{d}x_2 \mathrm{d}x_1 = E\int_0^L \tfrac{t}{2}(\theta - u')v_2' \, \mathrm{d}x_1 \\ &= E\int_0^L -\tfrac{t}{2}(\theta - u')' v_2 \, \mathrm{d}x_1, \end{aligned}$$

whereas the linear functional (7) evaluates to

$$L(\boldsymbol{v}_1) = 0, \quad L(\boldsymbol{v}_2) = -ta\int_0^L v_2 \, \mathrm{d}x_1,$$

since the inner products $\boldsymbol{f}\cdot\boldsymbol{v}_1 = 0$, $\boldsymbol{f}\cdot\boldsymbol{v}_2 = -av_2$. Now, by standard arguments (see, e.g., [5, Chapter 8.1.2]), we may expect the weighted averages

$$\int_0^L \big[E\big((\theta - u') - \tfrac{t^2}{6}\theta''\big)\big]v_1 \,\mathrm{d}x_1 = 0,$$
$$\int_0^L \big[-\tfrac{Et}{2}(\theta - u')' + ta\big]v_2 \,\mathrm{d}x_1 = 0,$$

to actually hold pointwise, and thereby we identify the strong forms

$$\frac{Et}{2}\frac{\mathrm{d}}{\mathrm{d}x_1}\left(\frac{\mathrm{du}}{\mathrm{d}x_1} - \theta\right) = -ta, \tag{19}$$
$$\frac{Et^2}{6}\frac{\mathrm{d}^2\theta}{\mathrm{d}x_1^2} + E\left(\frac{\mathrm{d}u}{\mathrm{d}x_1} - \theta\right) = 0. \tag{20}$$

If substituting (20) into (19) we obtain the system of ODEs

$$\begin{cases} \dfrac{Et^3}{12}\dfrac{\mathrm{d}^3\theta}{\mathrm{d}x_1^3} = ta \\ \dfrac{\mathrm{d}u}{\mathrm{d}x_1} = \theta - \dfrac{t^2}{6}\dfrac{\mathrm{d}^2\theta}{\mathrm{d}x_1^2} \end{cases} \tag{21}$$

which relates closely to (15). To see this, set $I = t^3/12$, $f = ta$ in the first equation, and then for the second, observe that

$$\frac{EI}{A\kappa G} = \frac{t^2}{6\kappa},$$

by using $E/G = 2$, $A = wt = t$.

In conclusion, making appropriate assumptions on the kinematic and constitutive relations in (5), allows for reducing the weak formulation to 1D, by integrating along the thickness of the beam. We retrieve the equations of the Timoshenko beam theory, apart from an absent shear coefficient κ, which compensates for the shear stress not being uniform over the cross-section R (it has a parabolic shape). Experimental data for a rectangular R suggests how

$$\kappa = \frac{5(1+\nu)}{6+5\nu} = \frac{5}{6}, \quad \text{if } \nu = 0,$$

according to [8]. Note that (21) approaches (14) as $t \to 0$, i.e., this model corresponds exactly to the Bernoulli beam theory in the limiting case (just as (15) does).

Remark. We emphasize that the additional kinematic relations (17) imposed on the solution, actually means that it does not belong to our model hierarchy, and consequently, neither does the Timoshenko beam. However, (21) then suggests the thin domain approach, in our setting, to be a natural extension of the beam theories, with less constraints on the solution.

4 A Posteriori Error Estimate

We pose two auxiliary problems: Find $\boldsymbol{u}^\psi \in V_\phi^h \otimes V_\psi$ and $\boldsymbol{u}^\phi \in V_\phi \otimes V_\psi^h$ such that

$$a(\boldsymbol{u}^\psi, \boldsymbol{v}) = L(\boldsymbol{v}), \quad \forall \boldsymbol{v} \in V_\phi^h \otimes V_\psi, \tag{22}$$
$$a(\boldsymbol{u}^\phi, \boldsymbol{v}) = L(\boldsymbol{v}), \quad \forall \boldsymbol{v} \in V_\phi \otimes V_\psi^h, \tag{23}$$

where the tensor-product solutions are semi-discrete (exact in one variable and approximate in the other). We shall outline estimates of the total error in energy norm

$$\|\boldsymbol{e}\|_a = \|\boldsymbol{u} - \boldsymbol{u}^h\|_a := a(\boldsymbol{u} - \boldsymbol{u}^h, \boldsymbol{u} - \boldsymbol{u}^h)^{1/2},$$

which uncouple terms representing the effects of the discretization and model errors. For this purpose, we consider (22) and (23) separately, first observing that

$$\|\boldsymbol{u} - \boldsymbol{u}^h\|_a = \|\boldsymbol{u} - \boldsymbol{u}^\psi + \boldsymbol{u}^\psi - \boldsymbol{u}^h\|_a \leq \|\boldsymbol{u} - \boldsymbol{u}^\psi\|_a + \|\boldsymbol{u}^\psi - \boldsymbol{u}^h\|_a \tag{24}$$

by the triangle inequality. The terms of the right-hand side are bounded, which we motivate by studying $\boldsymbol{e}^\psi = \boldsymbol{u}^\psi - \boldsymbol{u}^h$. Let $\pi_h : V_\phi^h \otimes V_\psi \to V_\phi^h \otimes V_\psi^h$ be a standard nodal interpolation operator[1] (or the L_2-projection), and note that

$$\begin{aligned}\|\boldsymbol{u}^\psi - \boldsymbol{u}^h\|_a^2 = a(\boldsymbol{u}^\psi - \boldsymbol{u}^h, \boldsymbol{e}^\psi) &\overset{(25)}{=} a(\boldsymbol{u}^\psi - \boldsymbol{u}^h, \boldsymbol{e}^\psi - \pi_h \boldsymbol{u}^\psi) \\ &\overset{(11)}{=} L(\boldsymbol{e}^\psi - \pi_h \boldsymbol{u}^\psi) - a(\boldsymbol{u}^h, \boldsymbol{e}^\psi - \pi_h \boldsymbol{u}^\psi),\end{aligned}$$

using the energy orthogonality

$$a(\boldsymbol{u}^\psi - \boldsymbol{u}^h, \boldsymbol{v}) = 0, \quad \forall \boldsymbol{v} \in V_\phi^h \otimes V_\psi^h. \tag{25}$$

Elementwise integration by parts of the second term gives

$$\begin{aligned}\|\boldsymbol{u}^\psi - \boldsymbol{u}^h\|_a^2 = &\sum_{K \in \mathcal{T}_h} \int_K (\boldsymbol{f} + \operatorname{div}(\boldsymbol{\sigma}(\boldsymbol{u}^h)) \cdot (\boldsymbol{e}^\psi - \pi_h \boldsymbol{e}^\psi) \, \mathrm{d}\boldsymbol{x} \\ &+ \int_{\partial\Omega_\mathrm{N}} \boldsymbol{g} \cdot (\boldsymbol{e}^\psi - \pi_h \boldsymbol{e}^\psi) \, \mathrm{d}s \\ &- \sum_{K \in \mathcal{T}_h} \int_{\partial K} \boldsymbol{\sigma}(\boldsymbol{u}^h) \cdot \boldsymbol{n}_K \cdot (\boldsymbol{e}^\psi - \pi_h \boldsymbol{e}^\psi) \, \mathrm{d}s,\end{aligned}$$

for $\boldsymbol{n}_K$ being the outward unit normal of the element boundary. Since each $E \in \mathcal{E}_I^h$ is common to two elements, we may regroup terms as

$$\begin{aligned}\|\boldsymbol{u}^\psi - \boldsymbol{u}^h\|_a^2 = &\sum_{K \in \mathcal{T}_h} \int_K (\boldsymbol{f} + \operatorname{div}(\boldsymbol{\sigma}(\boldsymbol{u}^h)) \cdot (\boldsymbol{e}^\psi - \pi_h \boldsymbol{e}^\psi) \, \mathrm{d}\boldsymbol{x} \\ &+ \int_{\partial\Omega_\mathrm{N}} (\boldsymbol{g} - \boldsymbol{\sigma}(\boldsymbol{u}^h) \cdot \boldsymbol{n}) \cdot (\boldsymbol{e}^\psi - \pi_h \boldsymbol{e}^\psi) \, \mathrm{d}s \\ &+ \sum_{E \in \mathcal{E}_I^h} \int_E [\boldsymbol{\sigma}(\boldsymbol{u}^h) \cdot \boldsymbol{n}_E] \cdot (\boldsymbol{e}^\psi - \pi_h \boldsymbol{e}^\psi) \, \mathrm{d}s,\end{aligned}$$

where we define

$$[\boldsymbol{\sigma}(\boldsymbol{u}^h) \cdot \boldsymbol{n}_E](\boldsymbol{x}) := \lim_{\epsilon \to 0^+} \big((\boldsymbol{\sigma} \cdot \boldsymbol{n}_E)(\boldsymbol{x} + \epsilon \boldsymbol{n}_E) - (\boldsymbol{\sigma} \cdot \boldsymbol{n}_E)(\boldsymbol{x} - \epsilon \boldsymbol{n}_E) \big), \quad \boldsymbol{x} \in E,$$

[1] The existence of such an interpolant is guaranteed, since $\boldsymbol{v} \in V_\phi \otimes V_\psi \subset H^2$ by assumption, and thus has pointwise values (see [9, Chapter 5.3]).

to be the jump in traction across the element edge E with unit normal $\boldsymbol{n}_E$. Then, by means of Cauchy's inequality and suitable estimates of the interpolation error $\boldsymbol{e}^{\psi} - \pi_h \boldsymbol{e}^{\psi}$, following Johnson and Hansbo [7, Theorem 2.1], we eventually arrive at

$$\|\boldsymbol{u}^{\psi} - \boldsymbol{u}^h\|_a \leq C_1\big(\|hR_1(\boldsymbol{u}^h)\|_{L_2(\Omega)} + \|hR_2(\boldsymbol{u}^h)\|_{L_2(\Omega)}\big), \tag{26}$$

where

$$R_1(\boldsymbol{u}^h) = |\boldsymbol{R}_1(\boldsymbol{u}^h)|, \quad R_2(\boldsymbol{u}^h) = h^{1/2}\frac{\|\boldsymbol{R}_2(\boldsymbol{u}^h)\|_{L_2(\partial\Omega)}}{V(K)},$$

with $V(K)$ as the volume of K, and

$$\begin{aligned}
\boldsymbol{R}_1(\boldsymbol{u}^h) &= \boldsymbol{f} + \operatorname{div}(\boldsymbol{\sigma}(\boldsymbol{u}^h)), && \text{on } K,\ K \in \mathcal{T}_h,\\
\boldsymbol{R}_2(\boldsymbol{u}^h) &= \begin{cases} \frac{1}{2}[\boldsymbol{\sigma}(\boldsymbol{u}^h)\cdot\boldsymbol{n}_E]/h_K, & \text{on } E,\ E \in \mathcal{E}_I^h,\\ (\boldsymbol{g} - \boldsymbol{\sigma}(\boldsymbol{u}^h)\cdot\boldsymbol{n})/h_K, & \text{on } E,\ E \in \mathcal{E}_B^h. \end{cases}
\end{aligned}$$

$\boldsymbol{R}_1$ and $\boldsymbol{R}_2$ represent the residuals related to the interior and the boundary of each element, respectively, whereas C_1 is a bounded interpolation constant, typically computable by a finite dimensional eigenvalue problem, see, e.g., [7, Equation 2.9, Section 2.3]. In the same manner, with $\pi_h : V_\phi \otimes V_\psi \to V_\phi^h \otimes V_\psi$, using the orthogonality relation

$$a(\boldsymbol{u} - \boldsymbol{u}^{\psi}, \boldsymbol{v}) = 0, \quad \forall \boldsymbol{v} \in V_\phi^h \otimes V_\psi,$$

we obtain

$$\|\boldsymbol{u} - \boldsymbol{u}^{\psi}\|_a \leq C_2\big(\|hR_1(\boldsymbol{u}^{\psi})\|_{L_2(\Omega)} + \|hR_2(\boldsymbol{u}^{\psi})\|_{L_2(\Omega)}\big), \tag{27}$$

Then, by adding and subtracting $\boldsymbol{u}^{\phi}$ in (24), analogous arguments eventually lead to

$$\|\boldsymbol{u}^{\phi} - \boldsymbol{u}^h\|_a \leq C_3\big(\|hR_1(\boldsymbol{u}^h)\|_{L_2(\Omega)} + \|hR_2(\boldsymbol{u}^h)\|_{L_2(\Omega)}\big), \tag{28}$$

$$\|\boldsymbol{u} - \boldsymbol{u}^{\phi}\|_a \leq C_4\big(\|hR_1(\boldsymbol{u}^{\phi})\|_{L_2(\Omega)} + \|hR_2(\boldsymbol{u}^{\phi})\|_{L_2(\Omega)}\big). \tag{29}$$

We assume the residuals (27) and (29), from the semi-discrete spaces, to be smaller than their discrete counterparts (26) and (28), i.e.,

$$\|\boldsymbol{u} - \boldsymbol{u}^{\psi}\|_a = (1-\alpha)\|\boldsymbol{u}^{\psi} - \boldsymbol{u}^h\|_a, \quad \|\boldsymbol{u} - \boldsymbol{u}^{\phi}\|_a = (1-\beta)\|\boldsymbol{u}^{\phi} - \boldsymbol{u}^h\|_a,$$

for some $0 \leq \alpha,\, \beta \leq 1$. This, given $\alpha = \beta = 0$, implies

$$\|\boldsymbol{u} - \boldsymbol{u}^h\|_a \leq 2\|\boldsymbol{u}^{\psi} - \boldsymbol{u}^h\|_a, \quad \|\boldsymbol{u} - \boldsymbol{u}^h\|_a \leq 2\|\boldsymbol{u}^{\phi} - \boldsymbol{u}^h\|_a,$$

as upper bounds of the total error, in terms of the model and discretization errors, respectively. It follows directly

$$\|\boldsymbol{u} - \boldsymbol{u}^h\|_a \leq \|\boldsymbol{u}^{\psi} - \boldsymbol{u}^h\|_a + \|\boldsymbol{u}^{\phi} - \boldsymbol{u}^h\|_a, \tag{30}$$

or, with $C = C_1 + C_3$,

$$\|\boldsymbol{u} - \boldsymbol{u}^h\|_a \leq C\big(\|hR_1(\boldsymbol{u}^h)\|_{L_2(\Omega)} + \|hR_2(\boldsymbol{u}^h)\|_{L_2(\Omega)}\big), \tag{31}$$

which is an (completely discretized) a posteriori error estimate.

Remark. The computational mesh is subjected to geometrical anisotropy—the elements have different dimension in different directions (one element spans the thickness of the domain, so $h(\boldsymbol{x}) \to t$, as more elements are introduced; see Section 5.2 for details). The a posteriori error estimate (31) does not take this into account, but doing so may lead to sharper error bounds. An example indicating how to get improved estimates is discussed in [7, Section 2.4]. We did not pursue this here.

5 Implementation

5.1 Fundamental concepts

Using adaptivity requires some tools, e.g., a suitable norm in which the error $\boldsymbol{e} = \boldsymbol{u} - \boldsymbol{u}^h$ is measured. In Section 4 the focus was on the energy norm $\|\cdot\|_a = a(\cdot, \cdot)^{1/2}$, seeing $\boldsymbol{u}^h$ as the minimizer to $\|\boldsymbol{u} - \boldsymbol{v}\|_a$ over $V_\psi^h \otimes V_\psi^h$. Note how (8) states that $\boldsymbol{u}^h$, as compared to $\boldsymbol{u}$, has a larger potential energy. Hence, since $F(\boldsymbol{u})$ may be expressed in terms of the energy norm,

$$F(\boldsymbol{u}) = \tfrac{1}{2}a(\boldsymbol{u}, \boldsymbol{u}) - L(\boldsymbol{u}) = \tfrac{1}{2}a(\boldsymbol{u}, \boldsymbol{u}) - a(\boldsymbol{u}, \boldsymbol{u}) = -\tfrac{1}{2}\|\boldsymbol{u}\|_a^2,$$

the relation $\|\boldsymbol{u}^h\|_a \leq \|\boldsymbol{u}\|_a$ holds, so the computed strains $\boldsymbol{\varepsilon}(\boldsymbol{u}^h)$ are underestimated, and the numerical problem gets too stiff. In Section 4 we used the well-known energy orthogonality

$$a(\boldsymbol{e}, \boldsymbol{v}) = 0, \quad \forall \boldsymbol{v} \in V_\psi^h \otimes V_\psi^h, \tag{32}$$

stating how the error $\boldsymbol{e}$ is orthogonal to the subspace $V_\psi^h \otimes V_\psi^h$. Important relations involving the energy norm can be derived from (32), e.g., the best approximation property

$$\|\boldsymbol{u} - \boldsymbol{u}^h\|_a = \inf_{\boldsymbol{v}} \|\boldsymbol{u} - \boldsymbol{v}\|_a, \quad \boldsymbol{v} \in V_\psi^h \otimes V_\psi^h,$$

which implies any refined FE-solution $\boldsymbol{u}^i$ to have larger energy norm, i.e.,

$$\|\boldsymbol{u}^i\|_a \geq \|\boldsymbol{u}^{i-1}\|_a, \quad i = 1, 2, \ldots, \tag{33}$$

since we are solving a minimization problem with respect to a larger function space. Another relation is the equality

$$\begin{aligned} \|\boldsymbol{e}\|_a^2 &= a(\boldsymbol{u} - \boldsymbol{u}^h, \boldsymbol{u} - \boldsymbol{u}^h) = a(\boldsymbol{u}, \boldsymbol{u} - \boldsymbol{u}^h) - a(\boldsymbol{u}^h, \boldsymbol{u} - \boldsymbol{u}^h) \overset{(32)}{=} a(\boldsymbol{u}, \boldsymbol{u} - \boldsymbol{u}^h) \\ &= a(\boldsymbol{u}, \boldsymbol{u}) - a(\boldsymbol{u}, \boldsymbol{u}^h) \overset{(32)}{=} a(\boldsymbol{u}, \boldsymbol{u}) - a(\boldsymbol{u}, \boldsymbol{u}^h) - a(\boldsymbol{u}^h - \boldsymbol{u}, \boldsymbol{u}^h) \\ &= a(\boldsymbol{u}, \boldsymbol{u}) - a(\boldsymbol{u}^h, \boldsymbol{u}^h) = \|\boldsymbol{u}\|_a^2 - \|\boldsymbol{u}^h\|_a^2, \end{aligned} \tag{34}$$

which holds only in energy norm.

5.2 The element

In Section 2 we mentioned the nodal basis, and to elaborate, tensor-product Lagrangian finite elements were implemented. The basis functions are constructed by means of one-dimensional Lagrange polynomials

$$l_i^{n-1} = \frac{(x - x_1) \cdots (x - x_{i-1})(x - x_{i+1}) \cdots (x - x_n)}{(x_i - x_1) \cdots (x_i - x_{i-1})(x_i - x_{i+1}) \cdots (x_i - x_n)}, \quad i = 1, 2, \ldots, n, \tag{35}$$

and are complete up to the highest order term (including additional mixed terms).

In order to treat larger classes of element geometries, one usually considers (isoparametric) mappings from a reference element $\hat{K}$ to the physical elements K_i. Let $\hat{K}$ be the quadrilateral with local coordinates $-1 \leq \xi, \eta \leq 1$, for which basis functions can be written

$$\varphi_j(\xi,\eta) = \varphi_{IJ}(\xi,\eta) = l_I^{q_{x_1}}(\xi)\, l_J^{q_{x_2}}(\eta),$$

identifying each node j with an index pair (I, J), where $1 \leq I \leq q_{x_1}{+}1$ and $1 \leq J \leq q_{x_2}{+}1$. q_{x_*} corresponds to the polynomial degree of the approximation, and we set $q_{x_1} = 1$, $1 \leq q_{x_2} \leq 12$, meaning, e.g., that $\boldsymbol{u}^h$ is linear in x_1. The approximation in x_2, through the thickness of the domain, vary edgewise (restricted to 12:th order polynomials for practical reasons), suggesting that q_{x_2} globally is represented by a N_{ed}-vector $\boldsymbol{q}$, with elements q_i, $i = 1, \ldots, N_{\text{ed}}$. Note that each mesh $\mathcal{T}_h$ becomes associated with a particular model $\boldsymbol{q}_h$ (in the sequel, to ease notation, this shall be implicitly assumed).

Example. The polynomial approximation $\boldsymbol{q} = (1, 2)$, as shown in Figure 2, gives rise to the local basis functions

$$\begin{aligned}
\varphi_1(\xi,\eta) &= l_1^1(\xi)\, l_1^1(\eta) = \tfrac{1}{4}(1-\xi)(1-\eta) \\
\varphi_2(\xi,\eta) &= l_1^1(\xi)\, l_2^1(\eta) = \tfrac{1}{4}(1-\xi)(1+\eta) \\
\varphi_3(\xi,\eta) &= l_2^1(\xi)\, l_1^2(\eta) = \tfrac{1}{4}(1+\xi)\eta(\eta-1) \\
\varphi_4(\xi,\eta) &= l_2^1(\xi)\, l_2^2(\eta) = \tfrac{1}{2}(1+\xi)(1+\eta)(1-\eta) \\
\varphi_5(\xi,\eta) &= l_2^1(\xi)\, l_3^2(\eta) = \tfrac{1}{4}(1+\xi)\eta(1+\eta)
\end{aligned}$$

readily derived via (35).

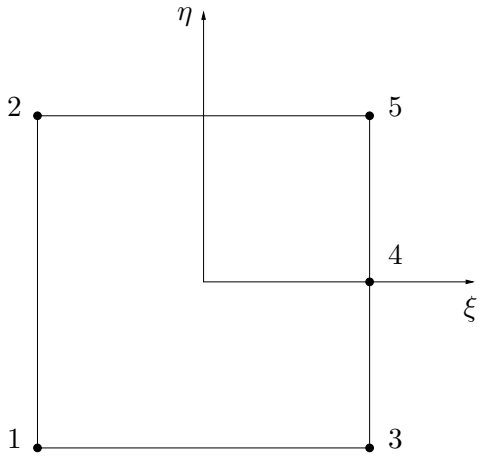

FIGURE 2: *Local node numbering for the 5-node quadrilateral* $\boldsymbol{q} = (1, 2)$

The domain Ω is partitioned into a conforming mesh, where the thickness t is spanned by a single element. Adjacent elements will overlap, leaving no hanging nodes. The discretization error e_{D}, related to the x_1-direction, is reduced when introducing more elements to the mesh. However, that does not resolve the model error e_{M} in x_2, which requires other means—instead

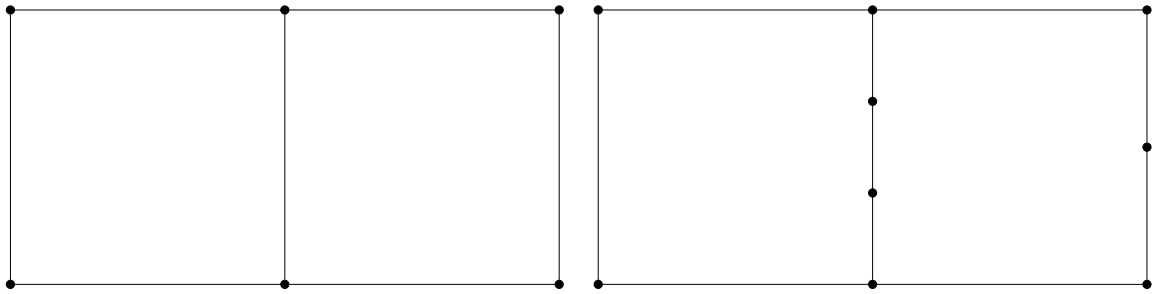

(A) *Simplest model using bilinear elements* (B) *Added complexity for* $\boldsymbol{q} = (1, 3, 2)$

FIGURE 3: *The model hierarchy is based on increasingly higher polynomial expansions*

convergence is obtained by increasing the polynomial degree of the interpolation along vertical edges. Examples of different model complexities for $N_{\text{el}} = 2$ is given in Figure 3.

Working with p-type FE-methods could impose restrictions on the choice of polynomial basis. Lagrangian finite elements have a potential caveat, as they tend to yield relatively dense stiffness matrices, subjected to bad conditioning. The better alternative would be to employ a well-conditioned modal hierarchical basis, represented by Legendre or Jacobi polynomials; we refer to [6, Chapter 1.1.5] for an introduction and further references.

Should cond($\mathbf{S}$) grow large, that indicates how the problem should be treated differently, e.g., by resorting to (full) elasticity theory. The numerical simulations in Section 5.4 managed without evident loss of accuracy[2].

5.3 Adaptive strategy

We opted for a residual-based approach, based on the idea that $\boldsymbol{u}^h$ does not satisfy (5) exactly, hoping to yield information about the error by exploiting this fact. Other common strategies—for error control in energy norm—include solving local Dirichlet or Neumann problems, and smoothening of discontinuous stresses by projection (known as the Zienkiewicz-Zhu method).

The adaptive procedure hinges on local error indicators identified via (30). We have

$$\begin{aligned} \|\boldsymbol{u}^\phi - \boldsymbol{u}^h\|_a^2 &= a(\boldsymbol{u}^\phi - \boldsymbol{u}^h, \boldsymbol{u}^\phi - \boldsymbol{u}^h) = a(\boldsymbol{u}^\phi, \boldsymbol{u}^\phi - \boldsymbol{u}^h) - a(\boldsymbol{u}^h, \boldsymbol{u}^\phi - \boldsymbol{u}^h) \\ &\overset{(23)}{=} L(\boldsymbol{u}^\phi - \boldsymbol{u}^h) - a(\boldsymbol{u}^h, \boldsymbol{u}^\phi - \boldsymbol{u}^h). \end{aligned} \tag{36}$$

Then (11), using $\boldsymbol{v} = \pi_n(\boldsymbol{u}^\phi - \boldsymbol{u}^h) = \pi_n \boldsymbol{u}^\phi - \boldsymbol{u}^h$, where $\pi_n : V_\phi \otimes V_\psi \to V_\phi^h \otimes V_\psi^h$ is a nodal interpolation operator, gives

$$L(\pi_n \boldsymbol{u}^\phi - \boldsymbol{u}^h) - a(\boldsymbol{u}^h, \pi_n \boldsymbol{u}^\phi - \boldsymbol{u}^h) = 0. \tag{37}$$

Adding (37) to (36) leads to

$$\|\boldsymbol{u}^\phi - \boldsymbol{u}^h\|_a^2 = L(\boldsymbol{u}^\phi - \pi_n \boldsymbol{u}^\phi) - a(\boldsymbol{u}^h, \boldsymbol{u}^\phi - \pi_n \boldsymbol{u}^\phi), \tag{38}$$

[2]The implemented Lagrangian finite element was not feasible for calculating reference solutions (cf. (45))

and analogously

$$\|\boldsymbol{u}^{\psi} - \boldsymbol{u}^{h}\|_a^2 = L(\boldsymbol{u}^{\psi} - \pi_n \boldsymbol{u}^{\psi}) - a(\boldsymbol{u}^{h}, \boldsymbol{u}^{\psi} - \pi_n \boldsymbol{u}^{\psi}), \tag{39}$$

representing the effects of the discretization and model errors. (The rationale behind (38) and (39), in the present context, are on the subtle side, since (36) gives equal estimates. Including the interpolant provides standard error estimates for further analysis.)

The functions $\boldsymbol{u}^{\phi}$ and $\boldsymbol{u}^{\psi}$ have to be discretized, and therefore we pose the problems: Find $\tilde{\boldsymbol{u}}^{\phi} \in V_{\phi}^{*} \otimes V_{\psi}^{h}$ and $\tilde{\boldsymbol{u}}^{\psi} \in V_{\phi}^{h} \otimes V_{\psi}^{*}$ such that

$$a(\tilde{\boldsymbol{u}}^{\phi}, \boldsymbol{v}) = L(\boldsymbol{v}), \quad \forall \boldsymbol{v} \in V_{\phi}^{*} \otimes V_{\psi}^{h}, \tag{40}$$

$$a(\tilde{\boldsymbol{u}}^{\psi}, \boldsymbol{v}) = L(\boldsymbol{v}), \quad \forall \boldsymbol{v} \in V_{\phi}^{h} \otimes V_{\psi}^{*}, \tag{41}$$

seeking enhanced FE-solutions as approximations. The function spaces $V_{\phi}^{*} \otimes V_{\psi}^{h}$ and $V_{\phi}^{h} \otimes V_{\psi}^{*}$ are defined with respect to $\mathcal{T}_h$: (40) is solved on a bisected mesh $\mathcal{T}_{\phi}$, having twice the number of elements as $\mathcal{T}_h$, with added vertical edges inheriting $\max\{q_i,\, q_{i+1}\}$ from the parent element K_i, exemplified by $\boldsymbol{q} = (1, 3, 2) \rightarrow (1, 3, 3, 3, 2)$ (the children retain the highest order term of the parental approximation). (41) is solved on a mesh $\mathcal{T}_{\psi}$, with the same number of elements as $\mathcal{T}_h$, but $q_i \rightarrow q_i + 1$ (all polynomial degrees along vertical edges are raised by 1), so that $\boldsymbol{q} = (1, 3, 2) \rightarrow (2, 4, 3)$. Since

$$\|\boldsymbol{u}^{\phi} - \boldsymbol{u}^{h}\|_a^2 = \sum_{i=1}^{N_{\mathrm{el}}} \|\boldsymbol{u}^{\phi} - \boldsymbol{u}^{h}\|_{a,\,K_i}^2,$$

(38) and (39) suggest the computable local error indicators

$$e_{\mathrm{D},\,K} = L(\tilde{\boldsymbol{u}}^{\phi} - \pi_n \tilde{\boldsymbol{u}}^{\phi})_K - a(\boldsymbol{u}^{h}, \tilde{\boldsymbol{u}}^{\phi} - \pi_n \tilde{\boldsymbol{u}}^{\phi})_K, \tag{42}$$

$$e_{\mathrm{M},\,K} = L(\tilde{\boldsymbol{u}}^{\psi} - \pi_n \tilde{\boldsymbol{u}}^{\psi})_K - a(\boldsymbol{u}^{h}, \tilde{\boldsymbol{u}}^{\psi} - \pi_n \tilde{\boldsymbol{u}}^{\psi})_K, \tag{43}$$

where assessing (43) typically requires less degrees of freedom, but also yields a denser stiffness matrix $\mathbf{S}$, due to more connections between neighbors (cf. *computational cost* below). In each iteration a fixed ratio r of the local error indicators—the largest absolute values regardless of error source—have their corresponding elements marked for refinement (neighbors subjected to model refinement have q_i raised by 1 on common edges). Notice that this direct comparison of local indicators is justified by (30).

The approach is straightforward, benefits from controlling the sizes[3] of the refined mesh and model, but becomes insensitive to presence of local singularities (then tends to overrefine). Any initial mesh/model $\mathcal{T}_0$ should not be too coarse (typically we want the error to fall within the asymptotic convergence rate of the error produced by pure h-refinement).

The reliability of the local error indicators is validated by the effectivity index

$$\theta = \frac{\left(\sum e_{\mathrm{D},\,K}\right)^{1/2} + \left(\sum e_{\mathrm{M},\,K}\right)^{1/2}}{\|\boldsymbol{u} - \boldsymbol{u}^{h}\|_a} = \frac{e_{\mathrm{est}}}{\|\boldsymbol{e}\|_a}, \tag{44}$$

which ideally remains constant during the adaptive refinement, thus indicating the algorithm to converge with the same order as the underlying FE-method. If unknown, the exact solution

[3]The more sophisticated strategy would be to predict the actual mesh size and model required to achieve the prescribed accuracy.

$\boldsymbol{u}$ was approximated by a reference solution $\tilde{\boldsymbol{u}}$, which substitutes into the denominator of (44) as $\tilde{e} = \|\tilde{\boldsymbol{u}} - \boldsymbol{u}^h\|_a$. For that purpose we state the problem: Find $\tilde{\boldsymbol{u}} \in V^h \times V^h$ such that

$$a(\tilde{\boldsymbol{u}}, \boldsymbol{v}) = L(\boldsymbol{v}), \quad \forall \boldsymbol{v} \in V^h \times V^h, \tag{45}$$

where V^h is the space of piecewise continuous quadratic functions (which vanishes on $\partial\Omega_{\mathrm{D}}$). The reference solution was resolved on a dense uniform triangulation $\mathcal{T}_r$ ($N_{\mathrm{d}}(\mathcal{T}_r) = 5\ 254\ 146$).

Remark. We emphasize that (30) foremost is a motivation behind (42) and (43), i.e., selecting elements for refinement, rather than providing accurate error control. When approximating the semi-discrete solutions by (40) and (41), it follows from (33) and (34) that

$$\|\boldsymbol{u}^\phi - \boldsymbol{u}^h\|_a - \|\tilde{\boldsymbol{u}}^\phi - \boldsymbol{u}^h\|_a = \|\boldsymbol{u}^\phi\|_a^2 - \|\tilde{\boldsymbol{u}}^\phi\|_a^2 \geq 0 \implies \|\boldsymbol{u}^\phi\|_a \geq \|\tilde{\boldsymbol{u}}^\phi\|_a,$$

which means we may lose the upper bound quality of (30). (This property is ensured by (31) for an upper bound of the interpolation constant, but we get no information on how to update mesh and model. Also, since (31) employs Cauchy's inequality on each element, it could yield considerable overestimations.)

A crude—but implementation independent—estimate of the computational cost for solving the primal problem is

$$N_{\mathrm{d}}(\mathcal{T}_h) = 2\sum_{i=1}^{N_{\mathrm{ed}}} q_i + 2N_{\mathrm{ed}},$$

in terms of the number of degrees of freedom N_{d} (mesh dependent). The adaptive procedure involves solving two refined problems in each iteration, to the separate costs

$$\begin{aligned} N_{\mathrm{d}}(\mathcal{T}_\phi) &= N_{\mathrm{d}}(\mathcal{T}_h) + 2\sum_{i=1}^{N_{\mathrm{el}}} \max\{q_i, q_{i+1}\} + 2N_{\mathrm{el}}, \\ N_{\mathrm{d}}(\mathcal{T}_\psi) &= N_{\mathrm{d}}(\mathcal{T}_h) + 2N_{\mathrm{ed}}, \end{aligned}$$

where $N_{\mathrm{ed}} = N_{\mathrm{ed}}(\mathcal{T}_h)$, $N_{\mathrm{el}} = N_{\mathrm{el}}(\mathcal{T}_h)$. If assuming $|q_i - q_{i+1}| \leq 1$ we get

$$2\sum_{i=1}^{N_{\mathrm{el}}} \max\{q_i, q_{i+1}\} \leq \sum_{i=1}^{N_{\mathrm{el}}} (q_i + q_{i+1} + 1) < 2\sum_{i=1}^{N_{\mathrm{ed}}} q_i + N_{\mathrm{el}} = N_{\mathrm{d}}(\mathcal{T}_h) + N_{\mathrm{el}} - 2N_{\mathrm{ed}},$$

and thus the total cost becomes

$$N_{\mathrm{d}}(\mathcal{T}_\phi) + N_{\mathrm{d}}(\mathcal{T}_\psi) < 3\big(N_{\mathrm{d}}(\mathcal{T}_h) + N_{\mathrm{el}}\big), \tag{46}$$

about three times the primal cost of solving (11). Moreover, (46) does not include calculating the local error indicators, and hence the overall procedure is more expensive, even though the cost of solving (40) and (41) is larger.

As for stopping criterion, the adaptive algorithm, detailed in Algorithm 1, halted once the finest model was locally introduced, i.e., if any $q_i = q_{\max} = 11$ (the last polynomial degree is reserved for $\tilde{\boldsymbol{u}}^\psi$). This was done for purpose of evaluation—a user-specified tolerance TOL is used in practice.

The implementation utilized a direct sparse Cholesky solver [3, 4] for solving the matrix problem (12).

Algorithm 1: Adaptive scheme

Data: initial mesh $\mathcal{T}_0$
Result: FE-solution $\boldsymbol{u}^h$, internal energy $\|\boldsymbol{u}^h\|_a^2$, estimated total error e_{est}

Let $*$ denote either sub- and superscripts ϕ and ψ

for $j = 0, 1, \ldots$ **do**
  solve primal problem (11) for $\boldsymbol{u}^h$ on $\mathcal{T}_j$
  calculate internal energy $\|\boldsymbol{u}^h\|_a^2$
  solve refined problems (40) and (41) for $\tilde{\boldsymbol{u}}^*$ on $\mathcal{T}_*$
  for $i = 1, \ldots, N_{\text{el}}$ **do**
    calculate local error indicators $e_{\text{D},\,K_i}$ and $e_{\text{M},\,K_i}$ via (42) and (43)
  end
  estimate total error e_{est}
  mark elements for refinement (h, q or hq)
  if any $q_i = q_{\max}$ **then**
    break
  else
    refine mesh and model: $\mathcal{T}_j \to \mathcal{T}_{j+1}$
  end
end

5.4 Numerical results

Cantilever beam. Let Ω be the unit square $0 \leq x_1, x_2 \leq 1$, which is kept fixed at $x_1 = 0$, and subjected to a surface traction $\boldsymbol{g} = (0, -1)$ at $x_2 = 1$. The material parameters are $E = 1$ and $\nu = 0.3$. The domain is not typically thin, but the solution, according to [1, p. 2170], has the exact internal energy $\|\boldsymbol{u}\|_a^2 = 1.903697$, and makes a suitable reference.

The problem was solved adaptively for an initial configuration $N_{\text{el}} = 10$, $q_i = 3$ and $r = 0.15$. Consecutive updates of mesh and model, $\mathcal{T}_j \to \mathcal{T}_{j+1}$, $j = 0, 1, 2, \ldots$, were dominated by the model error. The finest local model was introduced after 9 iterations, when the overall model complexity corresponded to 58 % of the finest global model:

$$\%(\text{model}) = 100 \cdot \frac{N_{\text{d}} - \min(N_{\text{d}})}{\max(N_{\text{d}}) - \min(N_{\text{d}})},$$

where $N_{\text{d}} = N_{\text{d}}(\mathcal{T}_j)$. Extreme values relate to the present refinement level j, such that

$$\min(N_{\text{d}}) = N_{\text{d}}(\mathcal{T}_j;\, q_i = 1),\ \max(N_{\text{d}}) = N_{\text{d}}(\mathcal{T}_j;\, q_i = q_{\max}).$$

The refinements were concentrated at the clamped end $x_1 = 0$, coinciding with large stresses and strains, close to the points $\boldsymbol{x}_1 = (0, 1)$, $\boldsymbol{x}_2 = (0, 0)$. The accuracy of $\|\boldsymbol{u}_9^h\|_a$ came within 0.2 %, not possible for the bilinear approximation (the simplest model at hand), for which $\|\boldsymbol{u}^h\|_a^2 \lessapprox 1.559$. Figure 4 further advocates the benefits of model adaptivity: the successive FE-solutions were more accurate than those obtained by uniform triangular P^2-approximations (according to (45) for subsequent mesh sizes $h = \sqrt{5}/4,\ 1/2,\ \sqrt{5}/8,\ 1/4,\ \sqrt{5}/16$). We normally expect singularities to be difficult to resolve using higher-order polynomial interpolations (the

exact solution would not be differentiable). Therefore the small error is somewhat surprising—$\boldsymbol{u}^h$ still manages to capture the local behavior of $\boldsymbol{u}$ in the vicinity of $\boldsymbol{x}_1$ and $\boldsymbol{x}_2$. In [1] the refinement strategy was another (based on the Zienkiewicz-Zhu method, trying to predict the mesh size), employing a bilinear approximation (not in a thin domain setting); the energy was $\|\boldsymbol{u}^h\|_a^2 = 1.89289$ over 718 degrees of freedom. This is less accurate than our FE-solution, which, however, was superseded at 964 degrees of freedom. Figure 6(a) shows the local error

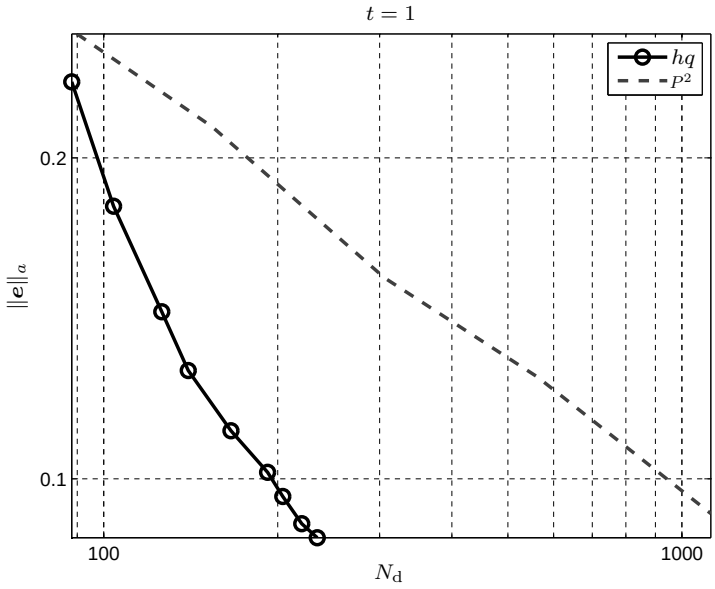

FIGURE 4: *Comparing model adaptivity (hq) and uniform triangular P^2-approximations*

contributions (40) and (41) to be of similar order, apart from a larger model error at $x_1 = 0$. The effectivity index θ, defined in (44), remained fairly constant, and judging by the data enclosed in Table 1, it also provides accurate error control. The triangle inequality leading to (24) approximately overestimated the total error by a factor $C \approx 1.3$-1.4

$$\|\boldsymbol{u} - \boldsymbol{u}^h\|_a = C\big(\|\boldsymbol{u} - \tilde{\boldsymbol{u}}^\phi\|_a + \|\tilde{\boldsymbol{u}}^\phi - \boldsymbol{u}^h\|_a\big),$$
$$\|\boldsymbol{u} - \boldsymbol{u}^h\|_a = C\big(\|\boldsymbol{u} - \tilde{\boldsymbol{u}}^\psi\|_a + \|\tilde{\boldsymbol{u}}^\psi - \boldsymbol{u}^h\|_a\big),$$

during the iterative procedure; alongside the FE-solutions $\tilde{\boldsymbol{u}}^\phi$ and $\tilde{\boldsymbol{u}}^\phi$ having smaller energy norms (as compared to their semi-discrete counterparts), that may, at least in some extent, account for $\theta \approx 1$.

Reducing the domain thickness ($t \to 1/10$) induced a shift towards h-refinement, suggesting how higher polynomial expansions are less important, when nature of the problem turns one-dimensional. The accuracy of $\|\boldsymbol{u}_{14}^h\|_a$—with respect to a reference solution $\|\tilde{\boldsymbol{u}}\|_a^2 = 1.903687$ (the surface traction was scaled, $\boldsymbol{g} = (0, -0.058582)$, to preserve the internal energy)—was less than 0.02 %, implying a linear improvement with respect to t. In Table 2 the data shows that 26.8 % of the finest model was used at the last refinement level, the first instance of q-refinement occurring at the 7:th iteration. Figure 6(b) indicates large variations in the model error at $x_1 = 0$, which suggests how the singularities cause problems after all (at least by being

TABLE 1: *Cantilever beam* ($t = 1$)

#iter	N_{d}	N_{el}	%(model)	cond($\mathbf{S}$)	$\|\boldsymbol{u}^h\|_a^2$	$\|\boldsymbol{e}\|_a$	θ
1	88	10	20.0	$2.02 \cdot 10^4$	1.848	$2.356 \cdot 10^{-1}$	0.941
2	104	11	23.3	$4.23 \cdot 10^4$	1.871	$1.802 \cdot 10^{-1}$	1.026
3	126	12	28.4	$1.05 \cdot 10^5$	1.883	$1.435 \cdot 10^{-1}$	1.013
4	140	12	33.9	$1.65 \cdot 10^5$	1.888	$1.264 \cdot 10^{-1}$	1.070
5	166	13	39.3	$2.92 \cdot 10^5$	1.891	$1.110 \cdot 10^{-1}$	1.061
6	192	14	44.0	$1.20 \cdot 10^6$	1.893	$1.015 \cdot 10^{-1}$	1.114
7	204	14	48.0	$2.56 \cdot 10^6$	1.894	$9.635 \cdot 10^{-2}$	1.128
8	220	14	53.3	$6.58 \cdot 10^6$	1.895	$9.086 \cdot 10^{-2}$	1.141
9	234	14	58.0	$1.64 \cdot 10^7$	1.896	$8.815 \cdot 10^{-2}$	1.146

difficult to resolve beyond a certain level). The discretization error is close to equidistributed, whereas the model error drops considerably away from the fixed end, which may be consistent with no local model refinements. The effectivity index was stable and accurate, the triangle inequality overestimating e_{T} roughly by a factor $C \approx 1.0$-1.4.

Figures 5(a) and 5(b) shows the FE-solutions for scaled displacements (due to large material deformations). Note the effects of shear deformations in the former.

TABLE 2: *Cantilever beam* ($t = 1/10$)

#iter	N_{d}	N_{el}	%(model)	cond($\mathbf{S}$)	$\|\boldsymbol{u}^h\|_a^2$	$\|\tilde{\boldsymbol{e}}\|_a$	θ
1	88	10	20.0	$2.13 \cdot 10^6$	1.395	$7.133 \cdot 10^{-1}$	0.826
2	112	13	20.0	$2.32 \cdot 10^6$	1.680	$4.725 \cdot 10^{-1}$	0.862
3	144	17	20.0	$3.31 \cdot 10^6$	1.780	$3.516 \cdot 10^{-1}$	0.901
4	192	23	20.0	$7.72 \cdot 10^6$	1.841	$2.515 \cdot 10^{-1}$	0.970
5	248	30	20.0	$9.42 \cdot 10^6$	1.865	$1.973 \cdot 10^{-1}$	0.990
6	320	39	20.0	$2.13 \cdot 10^7$	1.881	$1.524 \cdot 10^{-1}$	1.053
7	412	50	20.4	$3.01 \cdot 10^7$	1.890	$1.192 \cdot 10^{-1}$	1.023
8	526	63	21.1	$8.07 \cdot 10^7$	1.895	$9.532 \cdot 10^{-2}$	1.014
9	656	78	21.5	$1.52 \cdot 10^8$	1.898	$7.610 \cdot 10^{-2}$	1.002
10	842	97	23.0	$6.68 \cdot 10^8$	1.900	$6.125 \cdot 10^{-2}$	0.991
11	1062	122	23.2	$1.57 \cdot 10^9$	1.901	$5.019 \cdot 10^{-2}$	1.003
12	1352	153	23.9	$8.09 \cdot 10^9$	1.902	$4.000 \cdot 10^{-2}$	1.007
13	1708	189	25.0	$2.69 \cdot 10^{10}$	1.903	$3.281 \cdot 10^{-2}$	1.001
14	2154	229	26.8	$1.51 \cdot 10^{11}$	1.903	$2.785 \cdot 10^{-2}$	1.002

Varying Young's modulus. The domain is defined by $0 \leq x_1 \leq 1$, $0 \leq x_2 \leq 0.1$, completely fixed at both ends, and subjected to a surface traction $\boldsymbol{g} = (0, -1)$ at $x_2 = 0.1$. The material parameters are

$$E = \begin{cases} E_0 & x_1 \leq 0.5, \\ \alpha E_0 & \text{otherwise}, \end{cases}, \quad \text{for } E_0 = 100 \text{ and } \alpha = 10,$$

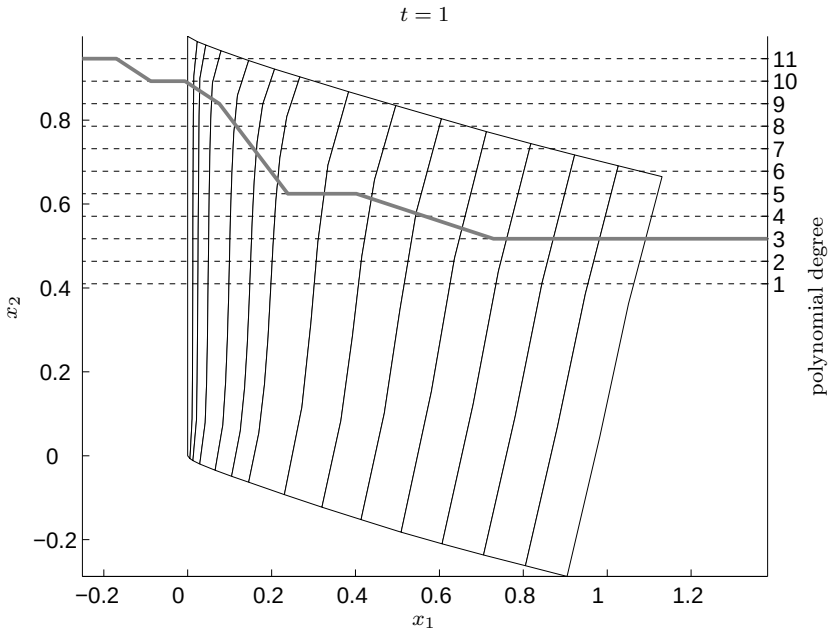

(A) *FE-solution* $\boldsymbol{u}_9^h$

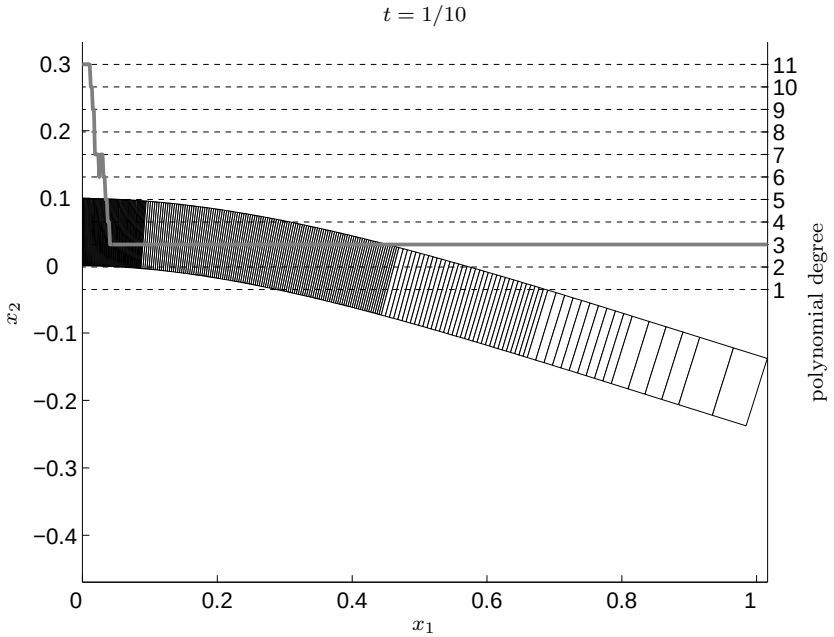

(B) *FE-solution* $\boldsymbol{u}_{14}^h$

FIGURE 5: *FE-solutions for cantilever beams of varying thicknesses*

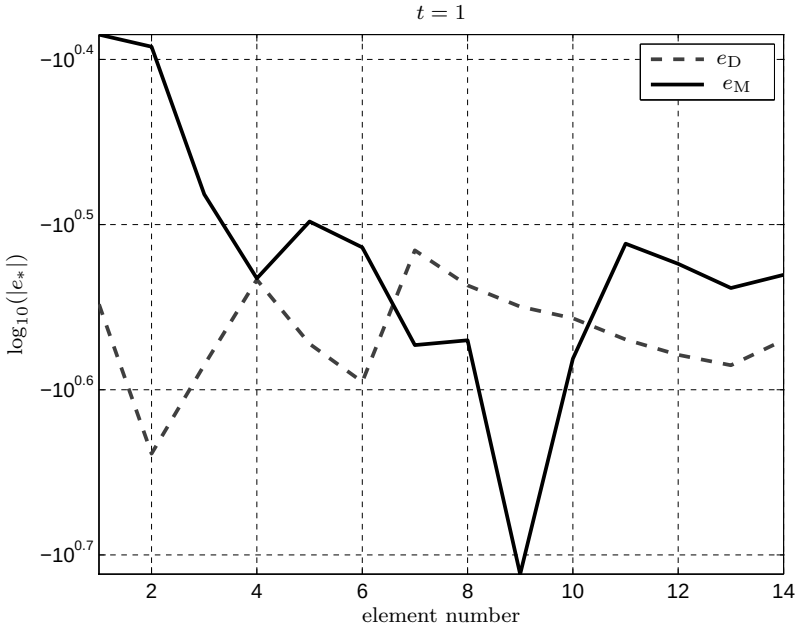

(A) *Error contributions for* $\boldsymbol{u}_9^h$

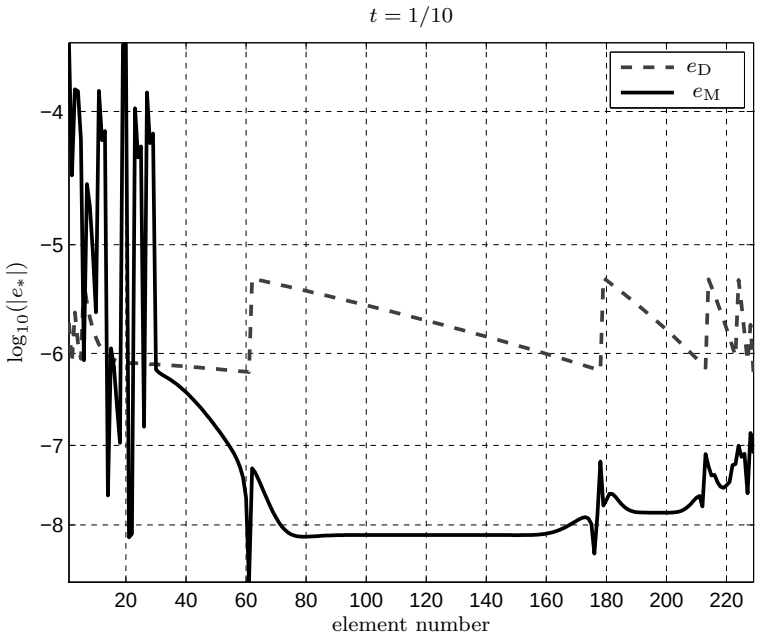

(B) *Error contributions for* $\boldsymbol{u}_{14}^h$

FIGURE 6: *Local error contributions at the last refinement levels*

whereas $\nu = 0$ (no lateral contraction), which then reduces $(\sigma_{11}, \sigma_{22}, \sigma_{12}) = E(\epsilon_{11}, \epsilon_{22}, \frac{1}{2}\epsilon_{12})$, without any coupling (the constitutive matrix $\boldsymbol{D}$ becomes diagonal). The internal energy was estimated $\|\tilde{\boldsymbol{u}}\|_a^2 \approx 0.069682$ with respect to $\mathcal{T}_r$.

The problem was solved for the initial configuration $N_{\text{el}} = 100$, $q_i = 3$ and $r = 0.15$, reaching an accuracy within 0.01 % at the 9:th refinement level, much improved over $\|\boldsymbol{u}^h\|_a^2 \lessapprox 0.068573$, obtained by using bilinear elements. Figure 7 shows a comparison between different refinement strategies (for hq, h and q), where solid lines indicate adaptive updates, and dashed ones mark uniform refinement (legend with subscript u). At the outset the problem is dominated by the discretization error (the q-methods hardly reduce the error), but subsequent introduction of additional elements makes the model error significant. The adaptive hq-strategy is the most accurate, converging with the same order as the corresponding uniform method. The model

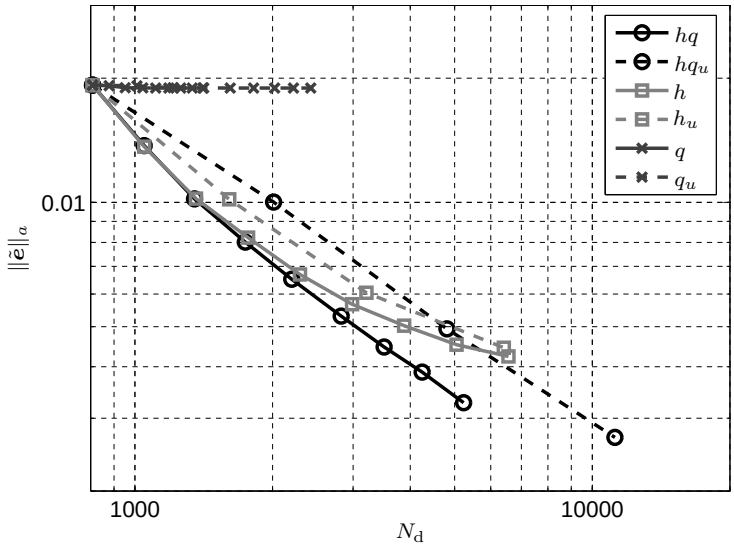

FIGURE 7: *Comparing refinement strategies*

refinements were concentrated at large variations in $\boldsymbol{\sigma} : \boldsymbol{\varepsilon}$, located about the center and at the clamped ends, visualized in Figures 9(a) and 9(b), using the norm

$$\|\boldsymbol{A}\| = (\boldsymbol{A} : \boldsymbol{A})^{1/2},$$

for the stress and strain tensors. In Figure 8(b) we note that large local model errors typically follow the same pattern, just as the error is small in regions without model refinements. The adaptive algorithm manages, more or less, to have local discretization errors of the same order. The effectivity index remained both stable and accurate (according to data in Table 3); the triangle inequality approximately overestimated e_{T} by a factor $C \approx 1.1$-1.4.

Figure 8(a) includes the graph of the analytical solution to the Bernoulli beam equation (centered in light gray)—alongside (2) the Bernoulli beam theory makes a simplified deformation relation, cf. Section 3. As the thickness of the domain decrease, in the current setting ($\nu = 0$), the potential energy (8) approaches that of the beam

$$F(u) = \frac{I}{2} \int_0^1 E(x) \left(u''(x)\right)^2 \, \mathrm{d}x - f \int_0^1 u(x) \, \mathrm{d}x,$$

TABLE 3: *Completely fixed console*

#iter	N_{d}	N_{el}	%(model)	cond($\mathbf{S}$)	$\|\boldsymbol{u}^h\|_a^2$	$\|\tilde{\boldsymbol{e}}\|_a$	θ
1	808	100	20.0	$5.33 \cdot 10^6$	0.069312	$1.642 \cdot 10^{-2}$	0.940
2	1048	129	20.3	$1.24 \cdot 10^7$	0.069493	$1.176 \cdot 10^{-2}$	1.024
3	1350	164	20.9	$3.25 \cdot 10^7$	0.069578	$8.663 \cdot 10^{-3}$	0.997
4	1744	210	21.3	$3.60 \cdot 10^7$	0.069617	$6.772 \cdot 10^{-3}$	1.017
5	2202	262	21.9	$5.33 \cdot 10^7$	0.069639	$5.460 \cdot 10^{-3}$	1.018
6	2826	323	23.6	$1.56 \cdot 10^8$	0.069654	$4.458 \cdot 10^{-3}$	1.064
7	3506	389	24.5	$2.65 \cdot 10^8$	0.069662	$3.708 \cdot 10^{-3}$	1.049
8	4246	466	25.5	$1.20 \cdot 10^9$	0.069667	$3.225 \cdot 10^{-3}$	1.077
9	5232	559	26.7	$3.98 \cdot 10^9$	0.069671	$2.704 \cdot 10^{-3}$	1.094

given by [10, Equation 15-74]. The exact potential is

$$F(u) = -\frac{(1+\alpha)\big(1+\alpha(254+\alpha)\big)}{3840E_0\alpha\big(1+\alpha(14+\alpha)\big)} \cdot \frac{f^2}{t^3} \approx -3.139155 \cdot 10^{-2},$$

and by a comparison, listed in Table 4, we conclude

$$\lim_{t\to 0^+} F(\boldsymbol{u}) = F(u),$$

implying that the suggested model hierarchy, in this sense, converges towards the Bernoulli beam (or rather the other way around). In Section 3 we showed equivalence for the limiting case with respect to a restriction of the simplest model.

Remark. The potential energy $F(\boldsymbol{u})$ was preserved by scaling of $\boldsymbol{g} = (0,\ f)$ (note that F is proportional to f^2/t^3); $F(\boldsymbol{u})$ was then approximated over adaptively refined dense meshes.

TABLE 4: *Comparing potentials*

t	$F(\boldsymbol{u})$	$F(\boldsymbol{u})/F(u)$
1/10	−0.0348408	1.1099
1/20	−0.0322466	1.0272
1/40	−0.0316050	1.0068
1/80	−0.0314454	1.0017
1/160	−0.0314038	1.0004
1/320	−0.0313959	1.0001

6 Conclusions

We summarize the results of the paper in the following list:

- The semi-discrete energy error estimate (30) provides a basis for an adaptive procedure, which, in the light of the examples in Section 5.4, seems not only reliable, but capable of sharp error control (which we have to admit is not obvious).
- The local error indicators (40) and (41) concentrated the updates of mesh and model to large variations in stresses and strains, i.e., at locations where we expect a predominant error.
- The accuracy of the FE-solutions were generally high, even when the physical domain had $L/t = 1$ (unit square), but we stress that this is not the typical thin domain setting. Refining the model adaptively was necessary to maintain efficiency; otherwise simpler models degenerate as $e_{\mathrm{D}} \to 0$.
- The suggested model hierarchy would be a natural extension to a larger hierarchy, by bridging the Bernoulli and Timoshenko beam theories with the (full) elasticity theory.

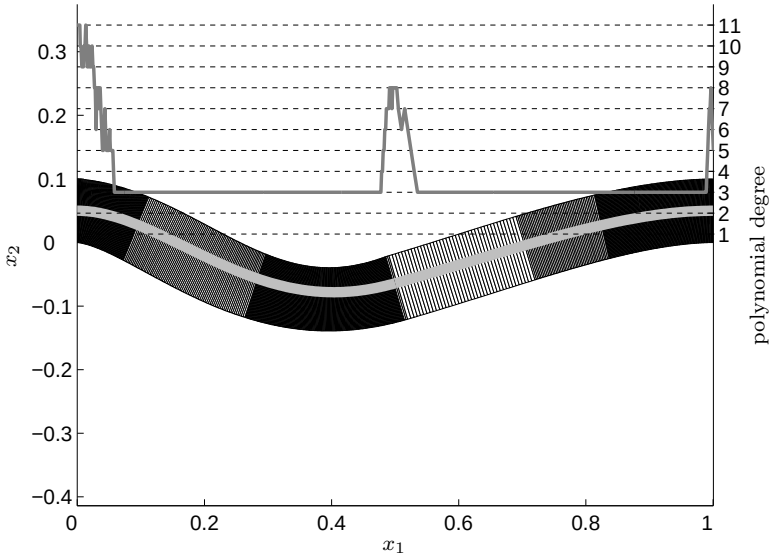

(A) *FE-solution* $\boldsymbol{u}_9^h$

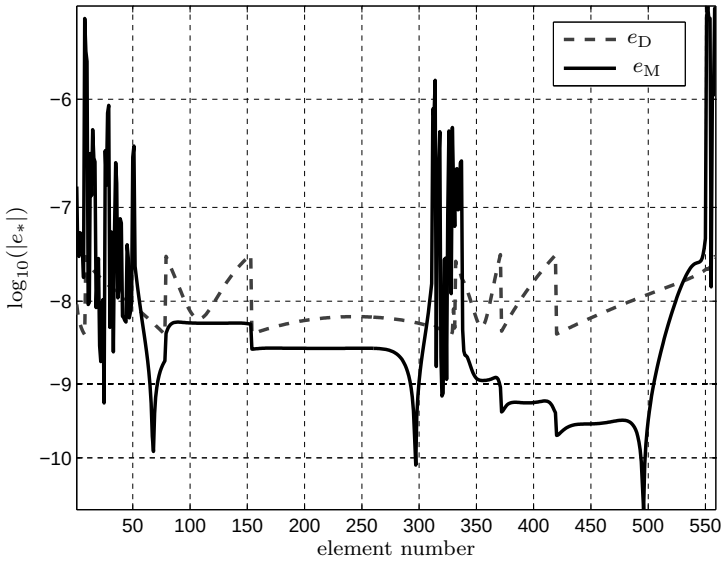

(B) *Local error contributions at last refinement level* $j = 9$

FIGURE 8: *Completely fixed console*

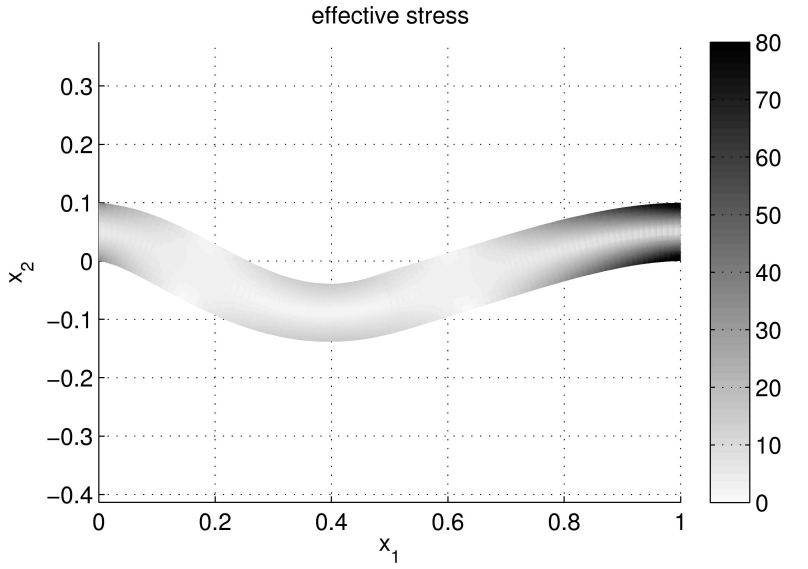

(A) *Large stresses located about* $x_1 = 1$

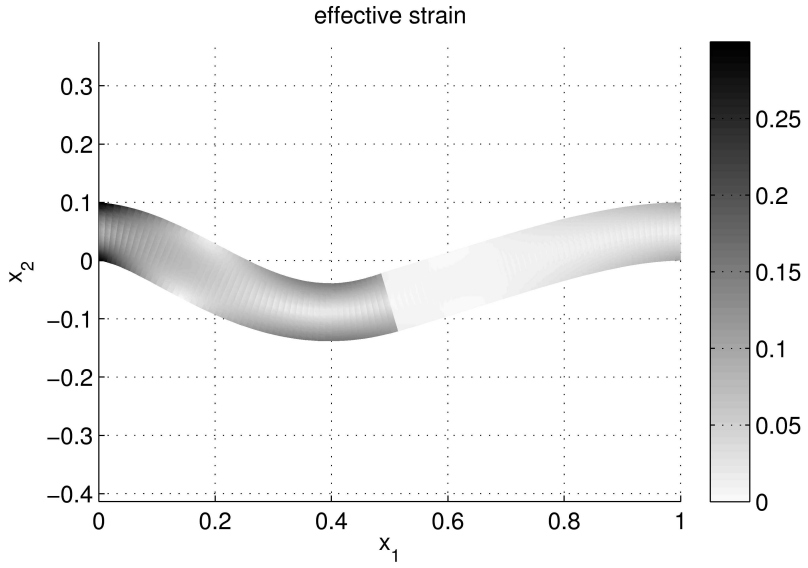

(B) *Large strains for* $0 \leq x_1 \leq 1/2$ *(where* E *is smaller)*

FIGURE 9: *Stresses and strains in the material*

References

[1] M. Ainsworth, J. Z. Zhu, A. W. Craig, and O. C. Zienkiewicz, *Analysis of the Zienkiewicz-Zhu a posteriori error estimator in the finite element method*, International Journal for Numerical Methods in Engineering **28** (1989), 2161–2174.

[2] I. Babuška, I. Lee, and C. Schwab, *On the a posteriori estimation on the modeling error for the heat conduction in a plate and its use for adaptive hierarchial modeling*, Applied Numerical Mathematics **14** (1994), 5–21.

[3] Yanqing Chen, Timothy A. Davis, William W. Hager, and Sivasankaran Rajamanickam, *Algorithm 887: CHOLMOD, Supernodal Sparse Cholesky Factorization and Update/Downdate*, ACM Transactions on Mathematical Software **35** (2008), no. 3.

[4] Timothy A. Davis and William W. Hager, *Dynamic Supernodes in Sparse Cholesky Update/Downdate and Triangular Solvers*, ACM Transactions on Mathematical Software **35** (2008), no. 4.

[5] K. Eriksson, D. Estep, P. Hansbo, and C. Johnson, *Computational differential equations*, Studentlitteratur, 1996.

[6] A. Ern and J-L. Guermond, *Theory and practice of finite elements*, Springer-Verlag, 2004.

[7] C. Johnson and P. Hansbo, *Adaptive finite element methods in computational mechanics*, Computer Methods in Applied Mechanics and Engineering **101** (1992), 143–181.

[8] T. Kaneko, *On Timoshenko's correction for shear in vibrating beams*, Journal of Physics D: Applied Physics **8** (1975), 1927–1936.

[9] S. Larsson and V. Thomeé, *Partial Differential Equations with Numerical Methods*, Springer-Verlag, 2003.

[10] H. Lundh, *Grundläggande hållfasthetslära*, 3:rd ed., Kungliga tekniska högskolan, 2000.

[11] N. S. Ottosen and H. Petersson, *Introduction to the finite element method*, Prentice Hall Europe, 1992.

[12] W. Weaver (JR), S. P. Timoshenko, and D.H. Young, *Vibration problems in engineering*, 5:th ed., John Wiley and Sons, 1990.